GCA - GEOCHIMICA et COSMOCHIMICA ACTA

TITLE: Experimental study on mafic rock dissolution rates within CO_2-seawater-rock systems

AUTHORS: Chiara Marieni[1*], Juerg M. Matter[1], Damon A. H. Teagle[1]

AFFILIATION:

[1] School of Ocean and Earth Science, National Oceanography Centre Southampton, University of Southampton, Southampton, SO14 3ZH, UK.

[*] **Corresponding author** now at: CNRS GET-UMR 5563, 14 Avenue Edouard Belin, 31400 Toulouse, France; Email: chiara.marieni@get.omp.eu

KEYWORDS:

Basaltic rocks; Ophiolitic rocks; Seawater dissolution rates; Carbon storage

Abstract

Far-from-equilibrium batch experiments have been performed to study the low temperature dissolution potential of crystalline submarine basalts (from Juan de Fuca Plate and Mid-Atlantic Ridges) and of a highly altered gabbro from the Troodos ophiolite (Cyprus) in presence of seawater and carbon dioxide (CO_2). The experiments have been carried out at 40 °C for up to 20 days with initial pH of ~4.8 and under ~1 bar pCO_2 to identify the progressive water-rock interactions. Elemental steady-state release rates from the rock samples have been determined for silicon and calcium, the solution concentrations of which were found to be the most effective monitors of rock dissolution. Mass balance calculations based on dissolved Si and Ca concentrations suggest the operation of reaction mechanisms focussed on the grain surfaces that are characteristic of incongruent dissolution. Also, basic kinetic modelling highlights the role of mass-transport limitations during the experiments. Ca release rates at pH ~5 indicate significant contributions of plagioclase dissolution in all the rocks, with an additional contribution of amphibole dissolution in the altered gabbro. Si release rates of all solids are found to be similar to previously studied reactions between seawater and basaltic glass and crystalline basalt from Iceland, but are higher than rates measured for groundwater-crystalline basalt interaction systems. This comparison with previous experimental results resumes the debate on the role of experimental variables, such initial rock mass and crystallinity, pCO_2, and fluid chemistry on dissolution processes. Our new data suggest that CO_2-rich saline solutions react with mafic rocks at higher rates than fresh water with low pCO_2, at the same pH. Most significantly, both ophiolitic gabbro and Juan de Fuca basalts show Si and Ca release rates similar or higher than unaltered crystalline basalt from Iceland, highlighting the potential substantial role that ophiolitic rocks and offshore mafic reservoirs could play for the geological storage of CO_2.

1. INTRODUCTION

Carbon dioxide (CO_2) is the principal greenhouse gas emitted into the atmosphere through human activities, and repeated warnings by the United Nations have emphasised the urgent need to minimise its effects on global climate and the environment (e.g., UN, 2015; IPCC, 2007; IPCC, 2014). One approach to curtail the increasing concentration of CO_2 in the atmosphere is the long-term storage of anthropogenically produced CO_2 within geologic reservoirs by converting gaseous CO_2 into carbonate minerals (e.g., Lackner et al., 1995; Seifritz, 1990; Sipilä et al., 2008). Carbon dioxide mineralization strongly depends on the availability of divalent cations, such as Ca^{2+}, Mg^{2+}, and Fe^{2+}, that once in contact with CO_2-rich fluids, can react with the bicarbonate (HCO_3^-) and carbonate (CO_3^{2-}) ions in solution to precipitate carbonate minerals, providing the permanent fixation of CO_2 as a stable solid mineral phase. Multiple experiments, numerical modelling, and pilot injection studies on CO_2 dissolution and precipitation suggest that mafic and ultramafic rocks such as seafloor basalts, which cover more than 60% of the Earth's surface, could supply both the required elevated cation content and the storage capacity (e.g., Dessert et al., 2003; Gadikota et al., 2014a; Gislason and Oelkers, 2014; Godard et al., 2011; Goldberg et al., 2008; Kelemen and Matter, 2008; Marieni et al., 2013;Matter and Kelemen, 2009; Oelkers et al., 2008),with mineral carbonation happening on the order of years (e.g., Gysi and Stefánsson, 2008; Matter et al., 2016; McGrail et al., 2016; Paukert et al., 2012; Rosenbauer et al., 2012; Schaef et al., 2010; Van Pham et al., 2012). Experimental approaches showing the high carbon removal potential of these rocks include studies on crystalline basalt and basaltic glass at low temperature (25 – 75 °C) (Clark et al., 2019; Galeczka et al., 2014; Gislason and Oelkers, 2003; Gudbrandsson et al., 2011; Gysi and Stefánsson, 2012a; Oelkers and Gislason, 2001), and at high temperature (75 -250 °C) (Gysi and Stefánsson, 2012b, c; Hellevang et al., 2017; Kumar et al., 2017; Marieni et al., 2018; Xiong et al., 2018); on metabasalt (Critelli et al., 2014); and on peridotite (Andreani et al., 2009; Kelemen and Matter, 2008). Based on measurements of silicon release rates, it has been observed that under specific conditions, such as low pH and high pCO_2, basalt dissolution rates may be nearly as high as those for olivine or peridotite (Matter and Kelemen, 2009; Wolff-Boenisch et al., 2011). Also, mineral dissolution rates in mafic and ultramafic rocks in presence of CO_2 have found to be enhanced by the increase of reactive surface area of the rock (e.g., Anbeek, 1992; Grandstaff, 1978), by increased temperatures (e.g., O'Connor et al., 2000), and by adding acids and bases (such as H_2SO_4, HNO_3, NaOH, and $NaHCO_3$) (e.g., Blum and Lasaga, 1988; Gadikota et al., 2014a; O'Connor et al., 2005; Oelkers, 2001; Teir et al., 2007). In addition, CO_2 geochemical trapping can be enhanced by dissolving the gas in water to facilitate the fluid-rock interactions and to limit the risk of CO_2 escaping back to the atmosphere due to the buoyancy of liquid or supercritical CO_2 (Gislason et al., 2010; Matter et al., 2016; McMillan and Bryant, 2009). In cases where fresh groundwater availability may be limited, solutions may lie in the use of seawater as the carbonation solution, for both on-land and offshore reservoirs. However, to date only a few experimental studies have focussed on reactions between CO_2-rich seawater solutions and basic rock types (Crovisier et al., 1987; Seyfried and Mottl, 1982; Wolff-Boenisch et al., 2011; Wolff-Boenisch and Galeczka, 2018), and, despite their vast occurrence on Earth, no dissolution experiments have been conducted using submarine basalts from the vast mid-ocean ridge flanks.

This study investigates the primary rock dissolution rates associated with low temperature CO_2 injections, mimicking the typical thermal conditions at oceanic ridge flanks, and evaluates the suitability of several mafic rock types as cation sources for potential CO_2 storage. Batch dissolution experiments have been carried out in a CO_2-seawater-mafic rock system at far-from equilibrium conditions, with a CO_2 partial pressure (pCO_2) of ~1 bar and 40 °C, using rocks from the upper oceanic crust and an ophiolitic gabbro.

2. MATERIAL AND METHODS

2.1. Reactive fluids

The artificial seawater used in the experiments (CaribSea Inc) has a salinity of ~35 psu, and the composition is in agreement with IAPSO seawater (Millero et al., 2008; Summerhayes and Thorpe, 1996) (Table 1). It was stored in the dark at 4 °C and warmed up to room temperature overnight prior to its use in the experiments.

Seawater pH was measured with a semi micro plastic BNC electrode (Fisherbrand^{TM}), connected to a pH meter (Accumet AB 15/15+, Fisher Scientific^{TM}). The electrode accuracy was calibrated against standard buffer solutions, with a standard deviation of 0.03 pH units. Total Alkalinity (TA) was determined with the Gran function using a modified titration methodology for a small-volume system (Haraldsson et al., 1997). Dissolved Inorganic Carbon (DIC) was calculated with the following equation (Grasshoff et al., 1999):

$$DIC = \frac{\mathrm{Ac}([\mathrm{H}^+]^2/K_1 + [\mathrm{H}^+] + K_2)}{[\mathrm{H}^+] + 2K_2} \tag{1}$$

with $[H^+]$ derived from pH, Ac (carbon Alkalinity) assumed equal to TA, and the dissociation constants $K_1 = 1.89 \times 10^{-6}$ and $K_2 = 1.85 \times 10^{-9}$ estimated for T = 40 °C, pCO_2 ~1 bar, and S = 35 psu, using the database available in Millero et al. (2006). The corresponding pCO_2 was calculated using Henry's Law for CO_2 solubility in water (Equation 2):

$$[CO_2] = K_0 * pCO_2 \tag{2}$$

where $[CO_2]$ is the aqueous CO_2 concentration in mol/L, and K_0 is Henry's constant. The aqueous CO_2 concentration was calculated from carbon alkalinity (Ac) as follows (Dickson et al., 2007):

$$[CO_2] = \frac{A_c}{(K_1/[H^+]) + (2 * K_1 * K_2/\,[H^+]^2)} \tag{3}$$

To determine K_0 at room temperature and 40 °C, the following expression proposed by Weiss (1974) was used:

$$\begin{gathered} lnK_0 = 9345.17/T - 60.2409 + 23.3585\ln(T/100) + S[0.023517 \\ -0.00023656T + 0.0047036(T/100)^2] \end{gathered} \tag{4}$$

where T is the temperature in Kelvin, and S is the salinity (35 psu).

The Si, Na, Mg, Ca, K, Sr and S concentrations in seawater were measured by inductively coupled plasma optical emission spectrometry (ICP–OES, Perkin-Elmer Optima 4300 DV) at the National Oceanography Centre Southampton. Precision of ICP–OES analyses based on repeated measurements of in-house standards is better than ± 3% for all the elements. Concentrations of SO_4 and Cl were measured by ion chromatography (IC, Dionex ICS2500). Repeat analysis of IAPSO seawater as well as single anion standards indicates that the precision of Cl and sulphate analyses is better than ±2% (Electronic supplement 1).

2.2. Rocks

The rocks used in this study are mid-ocean ridge basalts from the Juan de Fuca and Mid-Atlantic Ridges, and a gabbro from the Troodos ophiolite in Cyprus. The mineralogy was determined by optical microscopy of polished thin sections (Electronic supplement 2), and confirmed by scanning electron microscopy (SEM) analyses (Leo 1450VP SEM combined with Oxford Instruments X-Act 10 mm^2 area SDD EDS Detector).

The Juan de Fuca (JdF) samples consist of forty subsamples of 3.5 Ma crystalline basalt collected from the Hole U1362A during IODP Expedition 327 (Fisher et al., 2011). These rocks are heterogeneous multi-mineral solids that consist on average of 38 vol% labradoritic plagioclase, 23 vol% augitic clinopyroxene, 14 vol% mesostasis, 15 vol% secondary minerals, with minor olivine, magnetite, and glass. The secondary mineralogy is composed of Mg-saponite, celadonite, iron oxyhydroxides, and, where present, ~1 vol% calcite. This suite is typical of low temperature hydrothermal alteration, and is mainly associated with groundmass replacement, vesicle fill, and alteration halos (Fisher et al., 2011). Due to the small volume of individual specimen (~12 cm^3 each), they were combined together to form three composite samples based on textural differences and composition. These composite samples, corresponding to cryptocrystalline, microcrystalline, and fine grained basalts, are identified as “JdF mix 1”, JdF mix 2”, and “JdF mix 3”, respectively. Amongst these JdF basalts, the JdF mix 3 sample is characterised by the lowest volumetric abundance of labradoritic plagioclase (~32%).

The pillow basalt CD80WP132 from the Mid-Atlantic Ridge (MAR) was dredged from the Reykjanes Ridge, SW of Iceland, during the RRS Charles Darwin Cruise 80, at the Way Point 132 (28.66˚W, 60.54˚N) (Murton, 1995). The sample (MAR) is a vesicular cryptocrystalline olivine-bearing basalt consisting of 31 vol% labradoritic plagioclase, 20 vol% glass, 17 vol% augitic clinopyroxene, 11 vol% mesostasis, 6 vol% olivine, <1 vol% secondary minerals, and 15 vol% unfilled vesicles.

The gabbro from the Troodos ophiolite in Cyprus (G1) was sampled (at 32.93˚E, 34.93˚N) during fieldwork in May 2014, close to the village of Kato Amiandos. The medium-grained gabbro shows a high degree of hydrothermal alteration, with mineralogy consisting of 40 vol% anorthitic plagioclase, 40 vol% actinolitic amphibole almost completely replacing clinopyroxene (2 vol%), 13 vol% albitic plagioclase, 3 vol% chlorite, and 2 vol% talc.

All solids were crushed and ground to obtain the 63–125 µm size fraction, ultrasonically cleaned with multiple deionised water cycles of 5 minutes each to remove finer particles, and dried on a flat glass dish at 60 °C overnight in a vacuum oven. The chemical and mineralogical compositions of the 63–125 µm size fraction of each rock were determined by inductively coupled plasma mass spectrometry (ICP-MS, Thermo Scientific X-Series 2) on fully digested samples, and X-ray diffraction (XRD) (Electronic supplements 3 and 4, respectively). Furthermore, whole rock chemical analyses with X-ray fluorescence spectroscopy (XRF) were run at the University of St. Andrews (Scotland, UK; Table 2). In general, all the basaltic sample compositions within the range of mid ocean ridge basalt (MORB, see GERM, 2000).

The ground material was subjected to multiple physical analyses to constrain the grain size and morphology. The Brunauer-Emmett-Teller (BET) multipoint technique (Quantachrome NovaWin BET Analyzer via nitrogen, Columbia University, New York) was used to determine the surface areas of the rock samples. Resulting BET surface areas (A_{BET}) are listed in Table 3.

Specific geometric surface areas (A_{geo}) were also calculated assuming the grains are spherical (Equation 5):

$$A_{geo} = \frac{6}{(d \times \rho)} \tag{5}$$

where A_{geo} is the total area (cm^2/g), d the average particle diameter (cm), and ρ the density (g/cm^3) (Cubillas et al., 2005; Gautier et al., 2001; Guy and Schott, 1989; Wolff-Boenisch et al., 2004). Given that the abundance of clay and silt sized particles in the JdF samples will affect the average particle diameter, grain size distribution (GSD) and relative particle diameter average (d in Equation 5) were measured for each of the five samples using a Malvern Mastersize analyser (National Oceanography Centre Southampton). The samples were shaken overnight in a 0.05% Calgon solution to disaggregate the grains prior to analysis. The measured volumetric weighted means of particles were used to estimate average particle diameter and are reported with A_{geo} calculations in Table 3.

Between the two surface area measurements, A_{BET} and A_{geo}, the geometric surface area is considered by many studies to be more appropriate for estimating dissolution rates (Gautier et al., 2001; Wolff-Boenisch et al., 2004; Wolff-Boenisch et al., 2011). In this study, the calculated geometric surface areas were more consistent with the SEM observations of particle size than BET measurements carried out with nitrogen. For these reasons, the geometric rather than BET surface area will be considered in the following evaluations.

As for the bulk rocks, polished thin sections (PTS), and stubs were prepared for all the ground samples to further investigate and confirm the particle size distribution, composition and morphology by scanning electron microscopy.

2.3. Experimental setup

CO_2-water-rock batch experiments were carried out at 40 °C and pCO_2 ~1 bar in a three-phase system, consisting of ocean crust rocks, seawater and gaseous CO_2 in the headspace (Figure 1). The initial settings of all the eight runs are provided in Table 4. The five experiments JdF mix 1, 2, and 3, MAR-A (a subsample of MAR), and G1-A (a subsample of G1) are the runs with the highest initial rock mass (80 g), following the method of Gysi and Stefánsson (2012a) for moderate CO_2 concentrations. A portion (65 g) of the partially reacted rock used in each of the initial experiments with JdF mix 2 and MAR-A was used in follow-on experiments JdF mix 2bis and MAR-Abis, respectively. MAR-B is the experimental run with 30 g subsample of MAR. The series JdF mix 2bis, MAR-Abis, and MAR-B, characterized by different initial rock weight and by different fine particle abundance, were run to better quantify the role of reactive surface area and fine particles during dissolution. The JdF mix 2bis and MAR-Abis runs also provided information on the reactivity of the rocks during progressive dissolution experiments.

For each run, 4 fluorinated HDPE 1000 mL bottles were positioned in a 25 L stainless steel shaking water bath (MEDLINE BS-11). Each bottle was sealed with a Ley Rubber Ltd RB049/1H stopper with 4 holes: two of them for the inward and outward CO_2 flux; one for the pH electrode; and the last one served as a sampling port. In each bottle, 500 ± 10 mL of seawater were added and warmed to 40 °C. Once the temperature was reached, seawater was saturated with CO_2. The CO_2 flux from the 50 L cylinder was controlled by a standard gas regulator, and measured by a gas flowmeter. The CO_2 flux into each reaction bottle was further individually controlled with on/off gas valves (Swagelok®) positioned downstream of the flowmeter on each of the four gas lines. The CO_2 injection rate was set at 0.3 L/min. To homogeneously disperse the CO_2 (g) within the seawater, a stainless steel bubbler (0.5 µm pores) was positioned at the end of each gas line. The progressive oxidation of the bubbler was observed during the cleaning process, raising concerns about contamination from Fe in the experimental system. For this reason, Fe concentrations were not considered in our data analysis. The CO_2-saturation process was monitored through *in situ* regular pH measurements. For each pH measurement, the probe was inserted into the reaction vessel through a pre-made hole and then removed immediately after the value acquisition so that the exposure time of the electrode filling solution to CO_2 was minimised. Once seawater reached saturation with respect to dissolved CO_2 (1-3 days from the start of each experiment), 30 to 80 g of ground rock was added to each of the 3 bottles. These powders passively filled the base of the containers, and other than the shaking due to the movement of the water bath, the vessels were not stirred to avoid the formation of fine particles (e.g., Metz and Ganor, 2001).. The fourth bottle contained CO_2-saturated seawater without any rock, to provide a reference chemical composition throughout the duration of the experiments. After each run, bottles, tubing, and other materials used in the experiments were cleaned with 10% HNO_3 and then rinsed with ultrapure water.

Fluid samples were regularly collected from each bottle by opening the sampling ports one at the time, and temporarily closing the CO_2 gas line. For each sampling, 1 mL of solution was extracted with a plastic syringe: 0.5 mL was immediately analysed for alkalinity, whereas the other 0.5 mL was kept in the refrigerator for ICP-OES and IC analyses. To preserve the major cation content in the ICP-OES samples, a drop of concentrated sub-boiled HNO_3 was added. Considering the initial seawater volume, and an average total sampling volume of 12 mL, the original ratio between rock sample and water was not significantly modified.

2.4. Geochemical calculations

Aqueous absolute (Ca/Si) and relative (ΔCa/ΔSi) ratios have been calculated for all the collected fluid samples, to better characterise the reaction stoichiometry. The Ca/Si ratio expresses the elemental concentration variations with time, whereas the ΔCa/ΔSi ratio takes into account the initial solution composition, using:

$$\Delta Ca/\Delta Si = (Ca_x - Ca_0)/(Si_x - Si_0) \tag{6}$$

where “x” is the relative time in days, and “0” represents the initial concentration measured at time zero, just before adding the rock.

The reactivity of rocks has been determined at steady-state conditions for Ca and Si, which is defined as a condition where dissolution rates are time independent and where dissolution is stoichiometric (Oelkers, 2001). The elemental release rates have been calculated following the equation:

$$r_X = \log\left[(\Delta X * M_w)/(\mathrm{A} * M_r * t)\right] \tag{7}$$

where r_X is the release rate of element X expressed as log [mol/cm^2/s], ΔX the differential aqueous concentration of element X in mol/kg, M_w the water mass in kg at each sampling time, A the sample-specific surface area pre-experiment in cm^2/kg, M_r the original rock mass in kg, and t the elapsed time in seconds. A further attempt to determine the rock reactivity was made using the far-from-equilibrium dissolution rate proposed by Gislason and Oelkers (2003) for the kinetic calculations carried out with the PHREEQC program (Parkhurst and Appelo, 2013), via the recently developed thermodynamic database carbfix (Voigt et al., 2018) and the Si-Al basaltic glass phase defined by Galeczka et al. (2014). The potential moles of Si dissolved from the rock within CO$_2$-rich seawater in 10 days as a function of initial rock mass have been calculated as follows:

$$m_{Si} = A_a * exp^{-\left(\frac{Ea}{RT}\right)} * \left(\frac{a_{H^+}^3}{a_{Al^{3+}}}\right)^{\frac{1}{3}} * A * t \tag{8}$$

wherem_{Si} is the potential dissolved mole of Si, A_a a constant equal to 10$^{-5.6}$ (mol of Si)/cm^2/s, Ea the activation energy equal to 25.5 kJ/mol, R the gas constant in J/K/mol, T the absolute temperature in K, a_i the activity of the subscripted aqueous species, A the geometric surface area in cm^2/g, and t the elapsed time in s.

3. RESULTS

3.1. Fluid chemistry

The evolution of solution chemistry (pH, alkalinity, and DIC) as a function of time show similar compositional trends in all experiments (Figure 2). The composition of reference seawater solutions (blanks 2, 3, and 4) demonstrate how CO_2 saturation was reached at pH ~4.8, and alkalinity ~3.3 mM, with a slight oversaturation during the first day of experiment highlighted by the calculated DIC. In general, dissolved carbon concentrations were <40 mM. Experiments using rock powders show a rapid increase in pH and alkalinity during the first five days, from initial values of 4.6 and ~2.5 mM, to the maximum of 5.2 and ~5.0 mM, respectively. Because even the reference solutions showed increases in pH and alkalinity, the mass change was further investigated, weighing the bottles before and after each experiment. The analyses on the aqueous solutions (Electronic supplement 5) confirmed the progressive evaporation of seawater during the experiments, indicating mass losses of between 1 to 20% in each bottle. Assuming that chloride and sulphate are conserved, the concentrations of Na, Mg, Ca, K, Si and S in the fluids have been recalculated averaging the evaporation corrections from the IC data of chloride (Cl^-), and sulphate (SO_4^{2-}), and the ICP-OES data of total sulphur (S) analyses. The concentrations of Na, Mg, Ca, K, Sr and S have been corrected from the “initial saturation process” day, whereas Si concentrations only from the “rock addition” day because of the absence of silicon in the artificial seawater.

Amongst all the measured elements in solution, silicon and calcium show concentrations consistently increasing over time (Figure 3). Si is a key element in silicate mineral dissolution reactions, because it holds together the mineral framework (Oelkers, 2001). In addition, the absence of Si in the artificial seawater makes the chemical changes easier to detect in laboratory experiments. Nevertheless, Ca^{2+} is one of the divalent cations needed to precipitate CO_2 as a carbonate phase, and the determination of its release rate is essential to investigate the rock carbonation potential. Other dissolved ions are either present in very small quantities (e.g. Al), or do not show consistent variations in the solution with time (e.g., Na, Mg, and K). The Ca concentrations appear to reach steady-state after ~5 days, whereas Si concentrations continue to increase throughout the experiments (Figure 3). The Ca/Si stoichiometric ratio for basalts and gabbro used in these experiments is ~0.25, for reference seawater is ~100, whereas for artificial seawater used in the experiments is ~500 (Table 1). The Ca/Si ratio of artificial seawater is ~5 times higher than in reference seawater just because the overall low Si concentrations are slightly lower (0.02 and 0.10 mM, respectively), favouring the clear distinction of Si coming from the dissolution of the rocks.

3.2. Fine particles

Figure 4 shows GSD measurements, and the associated SEM images, for the samples before and after the experiments. The analyses of samples G1 and MAR confirm the absence of fine particles (<10 µm). In contrast, the JdF samples present a different scenario, with 16 to 40% in volume of particles less than 63 µm in the samples before the dissolution. Grain size analyses of the JdF samples following the first experimental runs measure lower clay-sized contents (2-5% by volume). This is partly due to the dissolution process during the experiment, and partially due to post-experiment cleaning cycles. Hence, given that the change in grain size is a critical parameter in the kinetic rate interpretation, particle diameters and corresponding geometric surface areas (A_{geo}) were measured and calculated, respectively, and repeated for samples that had already been used in previous experiments. Considering the GSD means, the particle diameters of JdF mix 2 increased from 42 µm (pre-experiment) to 74 µm (post-experiment), whereas GSD means were constant (~110 µm) for MAR-A. The calculated initial A_{geo} of JdF mix 2bis and MAR-Abis are then 279 and 188 cm^2/g, respectively (Table 3).

3.3. Rock dissolution

In these far-from equilibrium experiments, an almost constant pH is reached after five days in all the runs, and the rock stoichiometric dissolution is approached after 5-10 days. Considering the grain size distribution differences between the samples, the release rates have been normalized to the geometric surface area (Figure 5).

For the considered elements, Si and Ca, the corresponding release rates decrease with time. In general, Si release rates range from -13.2 to -14.1 log (mol/cm^2/s), whereas Ca release rates range from -12.3 to -14.1 log (mol/cm^2/s). The release rates for Si and Ca measured at the end of each experimental run are the closest to the stoichiometric dissolution, and range from -13.7 to -14.1 log (mol/cm^2/s), and from -13.3 to -14.1 log (mol/cm^2/s), respectively.

4. DISCUSSIONS

4.1. Effects of particle size on dissolution rates

The surface area available for reaction is one of the most important factors determining the reaction rate for a given rock volume, shape and time. Fine particles (<10 µm) have a higher ratio of surface area to volume, which in turn leads to higher dissolution rates. Consequently, the highest aqueous concentrations of Si and Ca shown by the JdF samples (Figure 3) are most probably related to their higher specific surface area, due to the abundance of very fine particles, in agreement with the observations in previous studies (Andreani et al., 2009; Beckingham et al., 2016; Gadikota et al., 2014b; Helgeson et al., 1984). However, the similarity among the calculated release rates of JdF fines-rich samples, and those of MAR and G1 fines-poor samples (Figure 5) confirms that the fastest kinetics related to fine particle abundance are accommodated by the surface area normalisation, enabling the appropriate comparison of samples. Overall, the strongly altered ophiolitic gabbro shows higher or similar surface area normalised release rates than the Jdf basalts. The MAR basalts are characterised by a wide range of release rates that are comparable or lower than JdF and gabbroic samples. There are no discernible changes in release rates associated with different degrees of crystallinity or grain size. The release rates of the medium-grained holocrystalline Troodos gabbro (G1) are similar to those of the more glassy MAR basalts and the cryptocrystalline JdF mix 1.

4.2. Effects of mass-transport limitations on dissolution rates Changes in the initial sample mass used during the experiments (from 80 to 30 g) did not significantly affect the Ca and Si concentrations in the final solutions (Figure 3). Therefore, the following hypothesis is proposed that the reactions are only occurring within the top-most layer of rock powder in the reactor due to mass-transport limitation caused by the experimental setup itself (Figure 6). In general, such mass-transport limitations arise when transport of reactants and/or products from/to the reaction sites (e.g. the water-rock interface) become the rate controlling reaction step, which can occur due to slow fluid advection or diffusion, or slow diffusion in the solid. If this hypothesis is true, the relative portion of dissolved rock, called dissolution extent, and the calculated elemental release rates will be higher, depending on the thickness of the top- layer that is reactive. An attempt has been made to quantify the top-layer weight using the far-from-equilibrium dissolution rate equation previously described (Equation 8), with normalization to geometric surface area.

The initial conditions of the experimental run “JdF mix 2bis” have been used together with the Si-Al basaltic glass phase (“Stapafell”) as the rock phase as model inputs. No precipitation was allowed, in agreement with what was observed during the experiments. The kinetic calculations show that ~5 g of Al-Si basaltic glass are enough to reach the experimental Si concentrations in solution, producing ~0.5 mmol/L of Si from the dissolution of less than 1% of the hypothesized total rock mass (<0.05 g). The extent of rock dissolution has then been estimated as a ratio between aqueous concentration difference and rock content, for both Si and Ca. Using measured XRF SiO_2 and CaO compositions of basalts and gabbro (Table 2), it is possible to estimate the maximum Si and Ca release, respectively, from the whole rock mass and from the top-layer only, and compare them with the actual ΔSi and ΔCa aqueous concentrations (Table 5). Calculations show that the average values of Si and Ca dissolution extent for the whole rock sample mass of 0.04% and 0.30%, respectively, would increase one order of magnitude if the reactions are only taking place within the top-layer (Table 5). The same order of magnitude difference is reflected by the elemental release rates (Figure 6).

A further mass-transport limitation is reflected by the incongruent dissolution within all the experimental runs. The extent of dissolution, as measured by Ca/Si ratios, decreases with rock dissolution progress, and approaches the whole rock Ca/Si stoichiometric ratio (~0.25), but without reaching it (Figure 3). These “non-stoichiometric” reactions may result from the formation of leached layers that are commonly an initial stage of the dissolution process (Oelkers, 2001). Previous observations on olivine dissolution show that the leaching of cations and incongruent mineral dissolution result in the formation of a Si-rich mass-transfer-limiting passivation layer, which eventually limits the extent of mineral dissolution (Béarat et al., 2006; Daval et al., 2011; Gadikota et al., 2014b). In this study, the formation of a passivation layer is suggested by evidence for incongruent dissolution and higher calcium release rates compared to Si (Figure 6). However, the close approach of Ca and Si release rates to the bulk rock Ca/Si ratio indicates that the fluid-rock exchange reactions are in the process of extending beyond the passivation layer, towards a more congruent dissolution. The same observation can be made from the ΔCa/ΔSi aqueous ratios (Figure 3), from which the artefacts due to the high cation content in seawater are removed. However, these preliminary considerations on mass-transport limitations have to be further tested and confirmed by additional experiments with different quantity of grains, and/or more vigorously agitated samples, to better constrain the rock mass exposed to dissolution.

4.3. Calcium source

The different aqueous calcium concentrations at pH ~5 from all the mafic rocks used during the experiments (Figure 3) can be used to determine which of the calcium-bearing phases are the most susceptible to dissolution. From previous experiments, calcite, glass and olivine are the most susceptible phases to dissolution, followed by pyroxene (diopside), amphibole, and plagioclase (e.g., Banfield et al., 1991; Crovisier et al., 1987; Eggleton et al., 1987). However, the alteration order of the last three minerals is not well established, because this depends on pH, temperature, and mineral composition (e.g., Fridriksson et al., 2001; Gudbrandsson et al., 2011; Nesbitt and Wilson, 1992). In general, for pH ~5, as measured in this experimental study, the kinetic calculations suggest that the mineral dissolution order is calcite > olivine and glass > anorthitic plagioclase > pyroxene > hornblendic amphibole > albitic plagioclase. The whole rock dissolution rates defined at 40 °C and pH 5 in this study are compared to dissolution rates of olivine, basaltic glass, plagioclase and pyroxene at 25 °C and pH 5 from the available literature. In general, mineral dissolution rates at 25 °C are up to ~0.5 log units slower than rates at 40 °C (Chen and Brantley, 1997; Knauss et al. 1993; Gislason and Oelkers, 2003; Rosso and Rimstidt, 2000; Schott et al. 1981).

Given the mineral average abundances within the samples used in this study (details in Electronic supplement 2), the Ca-bearing phases to be considered as potential Ca-sources from the basalts are mesostasis, labradoritic plagioclase, augitic pyroxene, and calcite, with the addition of glass for the MAR samples. In contrast, for the ophiolitic gabbro G1, the main Ca-bearing phases are amphibole, anorthitic plagioclase, and augitic pyroxene. The MAR basalts and JdF mix 3, do not show particularly high Ca release rates despite including 15-30% mesostasis and glass, and ~20% of pyroxene (Figure 5). In contrast, the JdF samples mix 1 and mix 2 – that have similar mesostasis, glass and pyroxene modal contents as the JdF mix 3 – and the ophiolitic gabbro G1 yield the highest release rates of Ca (-13.32, -13.48, and -13.59 log (mol/cm^2/s), respectively). This higher Ca-reactivity from the JdF mix 1 and mix 2 is too low to be explained by the presence of ~1% calcite, which is recognised in literature as very reactive (Cubillas et al., 2005), but could instead result from the dissolution of labradoritic plagioclase, which is less abundant in JdF mix 3 (~40% vs ~30%). Furthermore, the G1 has no calcite, and almost no clinopyroxene (~2%), so that the main mineral sources of Ca are amphibole and/or anorthitic plagioclase. There is no published experimental data on single-phase Ca release rates from amphiboles, but Si release rates from whole rock dissolution experiments at 25 °C of metabasalt with 50% of actinolite (Critelli et al., 2014) are slightly slower than our results even after compensating for the temperature effect (see below). On the other hand, several experiments have been carried out on plagioclase, although only a few have measured the Ca release rate directly (Berg and Banwart, 2000; Carroll and Knauss, 2005; Casey et al., 1991). Overall, these single-phase investigations demonstrate that the plagioclase dissolution rates increases with increasing anorthite content (Blum, 1994; Carroll and Knauss, 2005; Casey et al., 1991; Chou and Wollast, 1985; Gudbrandsson et al., 2014; Holdren and Speyer, 1987; Oelkers and Schott, 1995; Oelkers et al., 1994; Oxburgh et al., 1994; Stillings et al., 1996), for the pH range from 2 to 12 and temperatures up to 150 °C. Hence, the fast Ca release rates in the experimental runs with gabbro, JdF mix 1 and mix 2 are consistent with literature data on Ca-rich plagioclase, reflecting the high plagioclase abundance in the rocks, but does not exclude a Ca contribution from the amphibole in the ophiolitic gabbro. Also, the slower Ca release rates in the basalts (JdF mix 3 and MAR) can be related to the lower abundance of calcic plagioclase and/or to the lack of amphibole and calcite.

4.4. Comparison with literature

Among the experimental studies investigating fluid-rock interactions in CO_2-rich seawater, data from Wolff-Boenisch et al. (2011) are comparable to the current study results, due to similarities in the experimental setup (Table 6). Specifically, the initial values of the series "SWC-Cl" at 25 °C that studied the effect of the chemical components of seawater on dissolution rates are considered here because they represent the steady-state composition of the solution in the presence of basaltic glass, crystalline basalt, and peridotite. The Si release rates of SWC-Cl series as a function of pH are summarised in Figure 7, together with the elemental rates from all the experimental runs of this study, all normalized to geometric surface areas. The mafic rocks from Wolff-Boenisch et al. (2011), with basaltic glass included, exhibit significantly lower dissolution rates (~1 log unit) than the 25 °C dissolution curve described by Gislason and Oelkers (2003) for geometrically-normalized basaltic glass rates. The release rates of the oceanic rocks presented in this study are significantly lower than the 50 °C dissolution curve (Figure 7), being from less than 1 to ~2 log units lower in case of top-layer or whole rock mass assumptions, respectively. Hence, even though the major cation chemistries are relatively similar, discrepancies can be observed amongst the experimental sets of data and between experimental data and modelled curves. The explanations can be related to four crucial factors: mass-transport limitations, pCO_2, , fluid chemistry, and rock crystallinity (Table 6). The mass-transport limitations in the batch experiments of this study would explain the lowest release rates for the whole rock mass case, leaving the data from the top-layer option less than one log unit lower than the 50 °C dissolution curve from well mixed basaltic glass experiments. This is in agreement with the influence of experimental setups on measured release rates already observed by many authors (Clow and Drever, 1996; van Grinsven and van Riemsdijk, 1992), who measured higher rates with stirred ("mixed") batch reactors than with column experiments ("flow-through") or non-stirred batch reactors. The second factor potentially responsible for the rate discrepancies is the pCO_2. In the case of mixed-flow experiments, the 4 bar pCO_2 led to a pH of 3.5 and ~114 mM of dissolved inorganic carbon in solution (Wolff-Boenisch et al. 2011), which are ~1.5 and two orders of magnitude higher than for the batch experiments presented in this study, respectively. However, mixed-flow and top-layer batch experiments show a similar log unit discrepancy from the modelled curves for basaltic glass dissolution rates (at 25 and 50 °C, respectively) so that pCO_2 is interpreted to directly affect the pH, with higher H^+ activity resulting in higher cation release rates (Gislason and Oelkers, 2003; Wolff-Boenisch et al., 2004). This interpretation is supported by other experimental studies (e.g., Golubev et al., 2005) that found that silicate dissolution rates are weakly affected (±0.2 log units) by the presence of higher CO_2 concentration in solution, but are mainly driven by pH (H^+ activity).Fluid chemistry, with experiments run in presence of seawater and modelled curves based on fresh water systems (Table 6), could have inhibitory or catalytic effects on release rates. The catalytic effect of a number of acids and bases in solution (such as H_2SO_4, HNO_3, F^-, NaOH, and $NaHCO_3$) has been suggested by a number of studies (Gadikota et al., 2014a; O'Connor et al., 2005; Oelkers, 2001; Wolff-Boenisch, 2011). On the other hand, less conclusive interpretations have been obtained for the effect of ionic strength and NaCl contained in seawater on dissolution rates (Gadikota et al., 2014a; Gruber et al., 2019; Olsen et al., 2015; Wolff-Boenisch, 2011). Finally, to understand if crystallinity may play a role in the discrepancy between experiments and modelled curves, the Si release rate data in Figure 7 can be compared with the elemental release rates obtained by previous studies on crystalline phases (e.g., Figure 8: Critelli et al., 2014; Gudbrandsson et al., 2011). These authors carried out mixed-flow dissolution experiments on a metabasalt from an ophiolitic sequence (Monte Reventino, Italy), and a crystalline basalt from the Stapafell Mountain (SW-Iceland), respectively, to investigate the steady state elemental release rates in a CO_2-free aqueous solution (Table 6). The metabasalt consists of 50 vol% actinolitic amphibole, 32 vol% chlorite, 9 vol% epidote, 7 vol% albitic plagioclase, 1 vol% calcite, and 1 vol% phengite. The crystalline basalt used by Gudbrandsson et al. (2011) is the same as the crystalline basalt described by Wolff-Boenisch et al. (2011). Figure 7 shows that the Si release rates from this study calculated with the top-layer assumption are lower than the 50 °C basaltic glass dissolution curve (Gislason and Oelkers, 2003). However, Figure 8 shows that the same rates are higher than the elemental release rates measured for crystalline phases at 25 °C by Critelli et al. (2014), and Gudbrandsson et al. (2011) for pH ~5. A similar observation is apparent by comparing the Ca release rates, with the rates from the top-layer assumption from this study higher than the whole rock Ca release rates for crystalline basalt (Gudbrandsson et al., 2011) for a range of pH and temperatures (Figure 9). In particular, the actinolite-rich gabbro and the two Ca-plagioclase-rich JdF samples mix 1 and mix 2 show the highest Ca release rates. However, no further comparison can be made with other crystalline phases because plagioclase (Chou and Wollast, 1985; Gudbrandsson et al., 2011) and amphibole (Golubev et al., 2005) dissolution rates, as well as the data from Critelli et al. (2014), are normalized to BET rather than geometric surface area, which in general decreases the rates up to two order of magnitude, depending on grain roughness.

Hence, the rate differences can be related to mineralogy, as previously discussed, suggesting a major role of plagioclase in influencing Ca release rates, but also to mass-transport limitations, rock crystallinity, and solution composition. A catalytic effect of CO_2-rich seawater could explain the ~0.5 log unit difference at pH ~3.5 between the Si release rates measured by Wolff-Boenisch et al. (2011) and those by Gudbrandsson et al. (2011) (around -12.8 mol/cm^2/s), both obtained through mixed flow experiments on crystalline rocks, using the same apparatus in the same laboratory.

Further investigation on Si release rates of JdF, MAR, and G1 should be carried out with a variety of experimental setups, such as flow-through or stirred mixed-flow, varying pCO_2 values, and rock mass content, to have an improved perspective on their reactivity and to define the dependence on each experimental factor.

4.5. Implications for CO_2 sequestration sites

The CO_2 storage potentials in ocean crust basalt and ophiolitic gabbro have been investigated in this study with the aim of diversifying the environments of possible permanent CO_2 storage reservoirs.

The experimental runs conducted on offshore basalts (JdF and MAR samples) with CO_2-rich seawater simulate the low temperature hydrothermal circulation typical of mid-ocean ridge flanks, and focus on the rock dissolution processes. The results show cation release rates in agreement with previously proposed rates for terrestrial mafic rocks, which include both crystalline and basaltic glass, in particular if mass-transport limitation is taken into account. Our results suggest a ~0.5 log unit accelerating effect of seawater and/or pCO_2 on elemental release rates, but a decrease due to crystallinity in comparison to reactivity of amorphous phases. Moreover, the release rates determined in this study are comparable with the reactivity measured for the basaltic rocks involved in the CarbFix Project (Iceland), where the CO_2 captured from a geothermal power plant mineralised within the nearby basaltic formation in less than 2 years (Matter et al. 2016). Hence, this study not only confirms the capacity of seafloor basalts to dissolve relatively quickly, but also highlight the potential role of seawater and oceanic crust basalts for CO_2 sequestration offshore (Marieni et al., 2013). Given the significant porosity and permeability within the extrusive rocks of the ocean crust, the modern ocean floor presents a vast possible expansion of the suitable CO_2 geological storage. Furthermore, the aqueous results from the experimental run on the ophiolitic gabbro show how, from a geochemical perspectives, on-land rocks beyond basalts could be used as potential CO_2 reservoirs. However, the evolution of physical properties, such as porosity and permeability as a function of reaction progress still need to be addressed in order to quantify the exploitable potential of ophiolites for carbon sequestration.

5. CONCLUSIONS

Geochemical trapping of CO_2 in mafic and ultramafic rocks via CO_2 mineralization could be part of international carbon capture and storage mitigation strategies to reduce the growth rate of atmospheric CO_2 concentrations efficiently and permanently. The experimental work conducted in this study provides the first dissolution reaction data of basalts from the modern ocean floor, and gabbro from the Troodos ophiolite, in the presence of CO_2-rich seawater solutions. The elemental release rates for these rocks at low temperature (40 °C), and pCO_2 of ~1 bar have been determined from Si and Ca aqueous concentrations and range from -13.7 to -14.1 log (mol/cm^2/s), and from -13.3 to -14.1 log (mol/cm^2/s), respectively. Our experiments did not reach congruent dissolution in the elapsed time due to reactions focussed on the surface of mineral grains and, most probably, the formation of a passivation layer, enriched in Si and depleted in alkaline earth metals (e.g. Ca). The mass balance calculations based on Si and Ca concentrations and a basic kinetic model suggest that only the ~5 g top-layer of rock in the reaction vessel was actually involved in the reactions and providing the source for the dissolved ions. This highlights the need to identify the mass-transport limitation effects during experiments. The similarity of Si release rates of ophiolitic gabbro and basalts, the higher Ca release rate from the gabbro, JdF mix 1, and JdF mix 2, and the suggested catalytic effect of seawater and/or pCO_2 on mafic rock dissolution highlight the potential of ophiolitic and offshore rocks as CO_2 geological storage reservoirs.

Further investigations need to be carried out on seafloor and ophiolitic rocks to develop a more complete perspective on their reactivity and to define the extent of each experimental factors.

ACKNOWLEDGMENTS

We would like to thank Dr. M. Cooper, Dr. G. Gadikota, Dr. C. Menzies, Dr. J. Hunt, and Dr. R. Pearce for technical, analytical, and experimental assistance. Chiara Marieni was supported by a PhD scholarship from the University of Southampton Geochemistry Research Group. Additional funding for this research was provided by the Southampton Marine and Maritime Institute (SMMI) HEIF Research Collaboration Stimulus Funds to J.M. Matter and D.A.H. Teagle. DAHT also acknowledges support from NERC research grant (NE/I006311/1) and a Royal Society Wolfson Research Merit Award (WM130051).

APPENDIX A. SUPPLEMENTARY DATA

Supplementary data associated with this article can be found in the online version.

REFERENCES

Anbeek, C. (1992) Surface roughness of minerals and implications for dissolution studies. Geochimica et Cosmochimica Acta **56**, 1461-1469.

Andreani, M., Luquot, L., Gouze, P., Godard, M., Hoisé, E. and Gibert, B. (2009) Experimental study of carbon sequestration reactions controlled by the percolation of CO_2-rich brine through peridotites. Environmental Science & Technology **43**, 1226-1231.

Banfield, J.F., Jones, B.F. and Veblen, D.R. (1991) An AEM-TEM study of weathering and diagenesis, Abert Lake, Oregon: I. Weathering reactions in the volcanics. Geochimica et Cosmochimica Acta **55**, 2781-2793.

Béarat, H., McKelvy, M.J., Chizmeshya, A.V.G., Gormley, D., Nunez, R., Carpenter, R.W., Squires, K. and Wolf, G.H. (2006) Carbon Sequestration via Aqueous Olivine Mineral Carbonation: Role of Passivating Layer Formation. Environmental Science & Technology **40**, 4802-4808.

Beckingham, L.E., Mitnick, E.H., Steefel, C.I., Zhang, S., Voltolini, M., Swift, A.M., Yang, L., Cole, D.R., Sheets, J.M., Ajo-Franklin, J.B., DePaolo, D.J., Mito, S. and Xue, Z. (2016) Evaluation of mineral reactive surface area estimates for prediction of reactivity of a multi-mineral sediment. Geochimica et Cosmochimica Acta **188**, 310-329.

Berg, A. and Banwart, S.A. (2000) Carbon dioxide mediated dissolution of Ca-feldspar: implications for silicate weathering. Chemical Geology **163**, 25-42.

Blum, A.E. (1994) Feldspars in weathering, Feldspars and their reactions. Springer, pp. 595-630.

Blum, A.E. and Lasaga, A. (1988) Role of surface speciation in the low-temperature dissolution of minerals. Nature **331**, 431-433.

Carroll, S.A. and Knauss, K.G. (2005) Dependence of labradorite dissolution kinetics on CO_2(aq), Al(aq), and temperature. Chemical Geology **217**, 213-225.

Casey, W.H., Westrich, H.R. and Holdren, G.R. (1991) Dissolution rates of plagioclase at pH= 2 and 3. American Mineralogist (United States) **76**.

Chen, Y., and Brantley, S.L. (1997) Temperature- and pH-dependence of albite dissolution rate at acid pH. Chemical Geology **135**(3-4), 275-290.

Chou, L. and Wollast, R. (1985) Steady-state kinetics and dissolution mechanisms of albite. American Journal of Science **285**, 963-993.

Clark, D.E., Galeczka, I.M., Dideriksen, K., Voigt, M.J., Wolff-Boenisch, D. and Gislason, S.R. (2019) Experimental observations of CO2-water-basaltic glass interaction in a large column reactor experiment at 50 °C. International Journal of Greenhouse Gas Control **89**, 9-19.

Clow, D. and Drever, J. (1996) Weathering rates as a function of flow through an alpine soil. Chemical Geology **132**, 131-141.

Critelli, T., Marini, L., Schott, J., Mavromatis, V., Apollaro, C., Rinder, T., De Rosa, R. and Oelkers, E.H. (2014) Dissolution rates of actinolite and chlorite from a whole-rock experimental study of metabasalt dissolution from $2 \leq pH \leq 12$ at 25 °C. Chemical Geology **390**, 100-108.

Crovisier, J.L., Honnorez, J. and Eberhart, J.P. (1987) Dissolution of basaltic glass in seawater: Mechanism and rate. Geochimica et Cosmochimica Acta **51**, 2977-2990.

Cubillas, P., Köhler, S., Prieto, M., Chaïrat, C. and Oelkers, E.H. (2005) Experimental determination of the dissolution rates of calcite, aragonite, and bivalves. Chemical Geology **216**, 59-77.

Daval, D., Sissmann, O., Menguy, N., Saldi, G.D., Guyot, F., Martinez, I., Corvisier, J., Garcia, B., Machouk, I., Knauss, K.G. and Hellmann, R. (2011) Influence of amorphous silica layer formation on the dissolution rate of olivine at 90°C and elevated pCO_2. Chemical Geology **284**, 193-209.

Dessert, C., Dupré, B., Gaillardet, J., François, L.M. and Allègre, C.J. (2003) Basalt weathering laws and the impact of basalt weathering on the global carbon cycle. Chemical Geology **202**, 257-273.

Dickson, A.G., Sabine, C.L., Christian, J.R. (2007) Guide to best practices for ocean CO_2 measurements. North Pacific Marine Science Organization, 191pp. (PICES Special Publication 3). http://hdl.handle.net/11329/249.

Eggleton, R.A., Foudoulis, C. and Varkevisser, D. (1987) Weathering of basalt: changes in rock chemistry and mineralogy. Clays and Clay Minerals **35**, 161-169.

Fisher, A.T., Tsuji, T., Petronotis, K. and the Expedition 327 Scientists (2011) Proc. IODP, 327: Tokyo (Integrated Ocean Drilling Program Management International, Inc.).

Fridriksson, T., Neuhoff, P.S., Arnórsson, S. and Bird, D.K. (2001) Geological constraints on the thermodynamic properties of the stilbite-stellerite solid solution in low-grade metabasalts. Geochimica et Cosmochimica Acta **65**, 3993-4008.

Gadikota, G., Matter, J.M., Kelemen, P. and Park, A.-h.A. (2014a) Chemical and morphological changes during olivine carbonation for CO_2 storage in the presence of NaCl and $NaHCO_3$. Physical Chemistry Chemical Physics **16**, 4679-4693.

Gadikota, G., Swanson, E.J., Zhao, H. and Park, A.-H.A. (2014b) Experimental design and data analysis for accurate estimation of reaction kinetics and conversion for carbon mineralization. Industrial & Engineering Chemistry Research **53**, 6664-6676.

Galeczka, I., Wolff-Boenisch, D., Oelkers, E.H. and Gislason, S.R. (2014) An experimental study of basaltic glass–H_2O– CO_2 interaction at 22 and 50 °C: Implications for subsurface storage of CO_2. Geochimica et Cosmochimica Acta **126**, 123-145.

Gautier, J.-M., Oelkers, E.H. and Schott, J. (2001) Are quartz dissolution rates proportional to BET surface areas? Geochimica et Cosmochimica Acta **65**, 1059-1070.

GERM (2000) The Geochemical Earth Reference Model, http://EarthRef.org/agenda.htm.

Gislason, S.R. and Oelkers, E.H. (2003) Mechanism, rates, and consequences of basaltic glass dissolution: II. An experimental study of the dissolution rates of basaltic glass as a function of pH and temperature. Geochimica et Cosmochimica Acta **67**, 3817-3832.

Gislason, S.R. and Oelkers, E.H. (2014) Carbon storage in basalt. Science **344**, 373-374.

Gislason, S.R., Wolff-Boenisch, D., Stefansson, A., Oelkers, E.H., Gunnlaugsson, E., Sigurdardottir, H., Sigfusson, B., Broecker, W.S., Matter, J.M., Stute, M., Axelsson, G. and Fridriksson, T. (2010) Mineral sequestration of carbon dioxide in basalt: a pre-injection overview of the CarbFix project. International Journal of Greenhouse Gas Control **4**, 537-545.

Godard, M., Kelemen, P.B., Nasir, S. and Teagle, D.A.H. (2011) Geological carbon capture and storage in mafic and ultramafic rocks. Workshop, Muscat (Sultanate of Oman).

Goldberg, D.S., Takahashi, T. and Slagle, A.L. (2008) Carbon dioxide sequestration in deep-sea basalt. Proceedings of the National Academy of Sciences **105**(29), 9920-9925.

Golubev, S.V., Pokrovsky, O.S. and Schott, J. (2005) Experimental determination of the effect of dissolved CO_2 on the dissolution kinetics of Mg and Ca silicates at 25 °C. Chemical Geology **217**, 227-238.

Grandstaff, D.E. (1978) Changes in surface area and morphology and the mechanism of forsterite dissolution. Geochimica et Cosmochimica Acta **42**, 1899-1901.

Grasshoff, K., Kremling, K., Ehrhardt, M. (1999) Methods of seawater analysis, 3rd ed. Wiley-VCH, Weinhein, Germany, p. 600.Gudbrandsson, S., Wolff-Boenisch, D., Gislason, S.R. and Oelkers, E.H. (2011) An experimental study of crystalline basalt dissolution from $2 \leq pH \leq 11$ and temperatures from 5 to 75 ˚C. Geochimica et Cosmochimica Acta **75**, 5496-5509.

Gruber, C., Harlavan, Y., Pousty, D., Winkler, D. and Ganor, J. (2019) Enhanced chemical weathering of albite under seawater conditions and its potential effect on the Sr ocean budget. Geochimica et Cosmochimica Acta **261**, 20-34.

Gudbrandsson, S., Wolff-Boenisch, D., Gislason, S.R. and Oelkers, E.H. (2014) Experimental determination of plagioclase dissolution rates as a function of its composition and pH at 22 °C. Geochimica et Cosmochimica Acta **139**, 154-172.

Guy, C. and Schott, J. (1989) Multisite surface reaction versus transport control during the hydrolysis of a complex oxide. Chemical Geology **78**, 181-204.

Gysi, A.P. and Stefánsson, A. (2008) Numerical modelling of CO_2-water-basalt interaction. Mineralogical Magazine **72**, 55-59.

Gysi, A.P. and Stefánsson, A. (2012a) CO_2-water–basalt interaction. Low temperature experiments and implications for CO_2 sequestration into basalts. Geochimica et Cosmochimica Acta **81**, 129-152.

Gysi, A.P. and Stefánsson, A. (2012b) Experiments and geochemical modeling of CO_2 sequestration during hydrothermal basalt alteration. Chemical Geology **306–307**, 10-28.

Gysi, A.P. and Stefánsson, A. (2012c) Mineralogical aspects of CO_2 sequestration during hydrothermal basalt alteration - An experimental study at 75 to 250 °C and elevated pCO_2. Chemical Geology **306–307**, 146-159.

Haraldsson, C., Anderson, L.G., Hassellöv, M., Hulth, S. and Olsson, K. (1997) Rapid, high-precision potentiometric titration of alkalinity in ocean and sediment pore waters. Deep Sea Research Part I: Oceanographic Research Papers **44**, 2031-2044.

Helgeson, H.C., Murphy, W.M. and Aagaard, P. (1984) Thermodynamic and kinetic constraints on reaction rates among minerals and aqueous solutions. II. Rate constants, effective surface area, and the hydrolysis of feldspar. Geochimica et Cosmochimica Acta **48**, 2405-2432.

Hellevang, H., Haile, B.G. and Tetteh, A. (2017) Experimental study to better understand factors affecting the CO_2 mineral trapping potential of basalt. Greenhouse Gases: Science and Technology **7**, 143-157.

Hoffert, M.I., Caldeira, K., Benford, G., Criswell, D.R., Green, C., Herzog, H., Jain, A.K., Kheshgi, H.S., Lackner, K.S., Lewis, J.S., Lightfoot, H.D., Manheimer, W., Mankins, J.C., Mauel, M.E., Perkins, L.J., Schlesinger, M.E., Volk, T. and Wigley, T.M.L. (2002) Advanced technology paths to global climate stability: Energy for a greenhouse planet. Science **298**, 981-987.

Holdren, G.R. and Speyer, P.M. (1987) Reaction rate-surface area relationships during the early stages of weathering. II. Data on eight additional feldspars. Geochimica et Cosmochimica Acta **51**, 2311-2318.

IPCC (2007) Climate Change 2007: Synthesis Report. Contribution of Working Groups I, II and III to the Fourth Assessment Report of the Intergovernmental Panel on Climate Change, in: Core Writing Team, P., R.K. and Reisinger, A. (Ed.), IPCC. Geneva, Switzerland, p. 104.

IPCC (2014) Climate Change 2014: Impacts, Adaptation, and Vulnerability. Part A: Global and Sectoral Aspects. Contribution of Working Group II to the Fifth Assessment Report of the Intergovernmental Panel on Climate Change [Field, C.B., V.R. Barros, D.J. Dokken, K.J. Mach, M.D. Mastrandrea, T.E. Bilir, M. Chatterjee, K.L. Ebi, Y.O. Estrada, R.C. Genova, B. Girma, E.S. Kissel, A.N. Levy, S. MacCracken, P.R. Mastrandrea, and L.L. White (eds.)]. Cambridge University Press, Cambridge, United Kingdom and New York, NY, USA.

Kaszuba, J.P., Janecky, D.R. and Snow, M.G. (2005) Experimental evaluation of mixed fluid reactions between supercritical carbon dioxide and NaCl brine: Relevance to the integrity of a geologic carbon repository. Chemical Geology **217**, 277-293.

Kelemen, P.B. and Matter, J.M. (2008) In situ carbonation of peridotite for CO_2 storage. Proceedings of the National Academy of Sciences **105**, 17295-17300.

Knauss, K.G., Nguyen, S.N. and Weed, H.C. (1993) Diopside dissolution kinetics as a function of pH, CO_2, temperature, and time. Geochimica et Cosmochimica Acta **57**, 285-294.

Kumar, A., Shrivastava, J.P. and Pathak, V. (2017) Mineral carbonation reactions under water-saturated, hydrothermal-like conditions and numerical simulations of CO_2 sequestration in tholeiitic basalt of the Eastern Deccan Volcanic Province, India. Applied Geochemistry **84**, 87-104.

Lackner, K.S., Wendt, C.H., Butt, D.P., Joyce Jr, E.L. and Sharp, D.H. (1995) Carbon dioxide disposal in carbonate minerals. Energy **20**, 1153-1170.

Marieni, C., Henstock, T.J. and Teagle, D.A.H. (2013) Geological storage of CO_2 within the oceanic crust by gravitational trapping. Geophysical Research Letters **40**(23), 6219-6224.

Marieni, C., Přikryl, J., Aradóttir, E.S., Gunnarsson, I. and Stefánsson, A. (2018) Towards 'green' geothermal energy: Co-mineralization of carbon and sulfur in geothermal reservoirs. International Journal of Greenhouse Gas Control **77**, 96-105.

Matter, J.M. and Kelemen, P.B. (2009) Permanent storage of carbon dioxide in geological reservoirs by mineral carbonation. Nature Geoscience **2**(12), 837-841.

Matter, J.M., Stute, M., Snæbjörnsdottir, S.Ó., Oelkers, E.H., Gislason, S.R., Aradottir, E.S., Sigfusson, B., Gunnarsson, I., Sigurdardottir, H., Gunnlaugsson, E., Axelsson, G., Alfredsson, H.A., Wolff-Boenisch, D., Mesfin, K., Reguera, D.F., Hall, J., Dideriksen, K. and Broecker, W.S. (2016) Rapid carbon mineralization for permanent disposal of anthropogenic carbon dioxide emissions. Science **352**, 1312-1314.

McGrail, B.P., Schaef, H.T., Spane, F.A., Cliff, J.B., Qafoku, O., Horner, J.A., Thompson, C.J., Owen, A.T. and Sullivan, C.E. (2016) Field validation of supercritical CO_2 reactivity with basalts. Environmental Science & Technology Letters **4**(1), 6-10.

McMillan, B., and Bryant, S.L. (2009) Surface dissolution: Minimizing groundwater impact and leakage risk simultaneously. Energy Procedia, **1**(1), 3707-3714.

Metz and Ganor (2001) Stirring effect on kaolinite dissolution rate. Geochimica et Cosmochimica Acta **65**, 3475–3490.

Millero, F.J., Feistel, R., Wright, D.G. and McDougall, T.J. (2008) The composition of standard seawater and the definition of the reference-composition salinity scale. Deep Sea Research Part I: Oceanographic Research Papers **55**, 50-72.

Millero, F.J., Graham, T.B., Huang, F., Bustos-Serrano, H. and Pierrot, D. (2006) Dissociation constants of carbonic acid in seawater as a function of salinity and temperature. Marine Chemistry **100**, 80-94.

Murton, B.J. (1995) RRS Charles Darwin Cruise CD80, 01 Sep-01 Oct 1993. The PETROS Programme (PETRogenesis of Oblique Spreading). Wormley, UK, Institute of Oceanographic Sciences Deacon Laboratory, 77pp. (Institute of Oceanographic Sciences Deacon Laboratory Cruise Report 241).

Nesbitt, H.W. and Wilson, R.E. (1992) Recent chemical weathering of basalts. American Journal of Science **292**, 740-777.

O'Connor, W.K., Dahlin, D.C., Nilsen, D.N., Rush, G., Walters, R.P. and Turner, P.C. (2000) CO_2 storage in solid form: a study of direct mineral carbonation, 5th International Conference on Greenhouse Gas Technologies. Albany Research Center (ARC), Albany, OR, Cairns, Australia.

O’Connor, W.K., Dahlin, D.C., Rush, G.E., Gerdemann, S.J., Penner, L.R. and Nilsen, D.N. (2005) Final Report: Aqueous Mineral Carbonation—Mineral Availability, Pretreatment, Reaction Parametrics, And Process Studies. DOE/ARC-TR-04-002. Albany, OR: Office of Process Development, National Energy Technology Laboratory, Office of Fossil Energy, US Department of Energy.

Oelkers, E.H. (2001) General kinetic description of multioxide silicate mineral and glass dissolution. Geochimica et Cosmochimica Acta **65**, 3703-3719.

Oelkers, E.H. and Gislason, S.R. (2001) The mechanism, rates and consequences of basaltic glass dissolution: I. An experimental study of the dissolution rates of basaltic glass as a function of aqueous Al, Si and oxalic acid concentration at 25 °C and pH = 3 and 11. Geochimica et Cosmochimica Acta **65**, 3671-3681.

Oelkers, E.H., Gislason, S.R. and Matter, J.M. (2008) Mineral carbonation of CO_2. Elements **4**, 333-337.

Oelkers, E.H. and Schott, J. (1995) Experimental study of anorthite dissolution and the relative mechanism of feldspar hydrolysis. Geochimica et Cosmochimica Acta **59**, 5039-5053.

Oelkers, E.H., Schott, J. and Devidal, J.L. (1994) The effect of aluminum, pH, and chemical affinity on the rates of aluminosilicate dissolution reactions. Geochimica et Cosmochimica Acta **58**, 2011-2024.

Olsen, A.A., Hausrath, E.M. and Rimstidt, J.D. (2015) Forsterite dissolution rates in Mg-sulfate-rich Mars-analog brines and implications of the aqueous history of Mars. Journal of Geophysical Research: Planets **120**, 388-400.

Oxburgh, R., Drever, J.I. and Sun, Y.-T. (1994) Mechanism of plagioclase dissolution in acid solution at 25 °C. Geochimica et Cosmochimica Acta **58**, 661-669.

Parkhurst, D.L., Appelo, C.A.J. (2013) Description of Input and Examples for PHREEQC Version 3-A Computer Program for Speciation, Batch-reaction, One-dimensional Transport, and Inverse Geochemical Calculations. US Geological Survey Techniques and Methods, Book 6, pp. 497.

Paukert, A.N., Matter, J.M., Kelemen, P.B., Shock, E.L. and Havig, J.R. (2012) Reaction path modeling of enhanced in situ CO_2 mineralization for carbon sequestration in the peridotite of the Samail Ophiolite, Sultanate of Oman. Chemical Geology **330–331**, 86-100.Rimstidt, J.D., Brantley, S.L. and Olsen, A.A. (2012) Systematic review of forsterite dissolution rate data. Geochimica et Cosmochimica Acta **99**, 159-178.

Rosenbauer, R.J., Thomas, B., Bischoff, J.L. and Palandri, J. (2012) Carbon sequestration via reaction with basaltic rocks: geochemical modeling and experimental results. Geochimica et Cosmochimica Acta **89**, 116-133.

Rosso, J.J. and Rimstidt D.J. (2000) A high resolution study of forsterite dissolution rates. Geochimica et Cosmochimica Acta **64**(5), 797-811.

Schaef, H.T., McGrail, B.P. and Owen, A.T. (2010) Carbonate mineralization of volcanic province basalts. International Journal of Greenhouse Gas Control **4**, 249-261.

Schott, J., Berner, R.A., and Sjöberg, E.L. (1981) Mechanism of pyroxene and amphibole weathering: I. Experimental studies of iron-free minerals. Geochimica et Cosmochimica Acta, **45**, 2123-2135.

Seifritz, W. (1990) CO_2 disposal by means of silicates. Nature **345**.

Seyfried, W.E.J. and Mottl, M.J. (1982) Hydrothermal alteration of basalt by seawater under seawater-dominated conditions. Geochimica et Cosmochimica Acta **46**, 985-1002.

Sipilä, J., Teir, S. and Zevenhoven, R. (2008) Carbon dioxide sequestration by mineral carbonation Literature review update 2005–2007. Report VT 1, 2008.

Stillings, L.L., Drever, J.I., Brantley, S.L., Sun, Y. and Oxburgh, R. (1996) rates of feldspar dissolution at pH 3–7 with 0–8 mM oxalic acid. Chemical Geology **132**, 79-89.

Summerhayes, C.P. and Thorpe, S.A. (1996) Oceanography: an Illustrated Guide. Manson Publishing, London.

Teir, S., Revitzer, H., Eloneva, S., Fogelholm, C.-J. and Zevenhoven, R. (2007) Dissolution of natural serpentinite in mineral and organic acids. International Journal of Mineral Processing **83**, 36-46.

United Nations (2015). The Paris agreement. Report of the Conference of the Parties on its twenty-first session, held in Paris from 30 November to 13 December 2015.

van Grinsven, J.J.M. and van Riemsdijk, W.H. (1992) Evaluation of batch and column techniques to measure weathering rates in soils. Geoderma **52**(1-2), 41-57.

Van Pham, T.H., Aagaard, P. and Hellevang, H. (2012) On the potential for CO_2 mineral storage in continental flood basalts – PHREEQC batch- and 1D diffusion–reaction simulations. Geochemical Transactions **13**, 5-5.

Voigt, M., Marieni, C., Clark, D.E., Gíslason, S.R., Oelkers, E.H. (2018) Evaluation and refinement of thermodynamic databases for mineral carbonation. Energy Procedia **146**, 81-91.

Weiss, R.F. (1974) Carbon dioxide in water and seawater: the solubility of a non-ideal gas. Marine Chemistry **2**, 203-215.

Wolff-Boenisch, D. (2011) On the buffer capacity of CO_2-charged seawater used for carbonation and subsequent mineral sequestration. Energy Procedia **4**, 3738-3745.

Wolff-Boenisch, D. and Galeczka, I.M. (2018) Flow-through reactor experiments on basalt-(sea) water-CO_2 reactions at 90 °C and neutral pH. What happens to the basalt pore space under post-injection conditions? International Journal of Greenhouse Gas Control **68**, 176-190.

Wolff-Boenisch, D., Gislason, S.R., Oelkers, E.H. and Putnis, C.V. (2004) The dissolution rates of natural glasses as a function of their composition at pH 4 and 10.6, and temperatures from 25 to 74 °C. Geochimica et Cosmochimica Acta **68**, 4843-4858.

Wolff-Boenisch, D., Wenau, S., Gislason, S.R. and Oelkers, E.H. (2011) Dissolution of basalts and peridotite in seawater, in the presence of ligands, and CO_2: implications for mineral sequestration of carbon dioxide. Geochimica et Cosmochimica Acta **75**, 5510-5525.

Xiong, W., Wells, R.K., Horner, J.A., Schaef, H.T., Skemer, P.A. and Giammar, D.E. (2018) CO_2 Mineral Sequestration in Naturally Porous Basalt. Environmental Science & Technology Letters **5**, 142-147.

TABLES

Table 1: Chemical composition of the starting solution for the experimental work. Values are given in mM.

	pH / °C	**TA**	**DIC**	**Si**	**Na**	**Mg**	**Ca**	**K**	**S**	**SO_4**	**Cl**
IAPSO reference*	8.10 / 20	2.30	1.94	0.10	469	53.1	10.3	10.2	28.2	28.2	546
IAPSO measured	7.66 / 20	2.38	2.23	0.11	468	52.6	10.5	10.0	28.1	27.5	555
SEAWATER measured	7.46 / 20	2.43	2.36	0.02	469	50.6	10.5	10.1	28.7	28.5	565

* from Summerhayes and Thorpe (1996), and Millero et al. (2008)

Table 2: Rock chemical compositions for 63-125 µm size fraction, measured with XRF analyses, and expressed in percent. Negative LOI values are most probably due to gain in mass due to oxidation of Fe^{2+} to Fe^{3+}. International standard OU-6 was used to test for accuracy (in general ≤2%; for P_2O_5, Na_2O, MgO < 11%), and precision (in general < 1%; for P_2O_5, Na_2O, MgO < 5%).

ID	SiO_2	TiO_2	Al_2O_3	FeO_{tot}	MnO	MgO	CaO	Na_2O	K_2O	P_2O_5	SO_3	LOI	TOT
JdF mix 1	49.6	1.93	13.6	11.7	0.23	6.47	12.4	2.35	0.20	0.15	0.10	1.33	100
JdF mix 2	48.6	1.66	13.7	11.2	0.20	7.40	13.9	2.15	0.12	0.07	0.13	0.93	100
JdF mix 3	50.1	1.70	13.7	11.6	0.20	6.79	12.9	2.12	0.18	0.06	0.08	0.58	100
MAR	49.0	1.24	12.5	14.5	0.22	7.65	12.9	1.70	0.03	0.05	0.24	-0.18	99.8
G1	44.9	0.09	17.2	5.54	0.11	11.1	17.1	0.95	0.04	<0.01	<0.03	2.70	99.7

Table 3: Surface areas measured with BET (A_{BET}) and geometrically calculated (A_{geo}) for each sample. Volumetric weighted means measured with Mastersizer and used as particle diameter averages in the A_{geo} calculations are shown. Density is assumed to be 2.9 g/cm^3 for all the samples.

	A_{BET} (cm^2/g)	A_{geo} (cm^2/g)	**Volumetric weighted mean of particles** (µm)
JdF mix 1	57240	406	51
JdF mix 2	123420	489	42
JdF mix 2bis		279	74
JdF mix 3	8760	781	27
MAR	22140	188	110
Mar Abis		188	110
G1	12670	191	108

Table 4: Summary of the initial conditions for the CO_2-seawater-oceanic rock dissolution experiments. The experimental runs containing only seawater (“blanks”), and used as reference to monitor the effect of rocks in solution, are shown at the top of each run series.

		Initial conditions						Saturated conditions at 40 °C			
	Total Duration	**T**	**pH / 40°C**	**TA**	**DIC**	**pCO_2**	**Saturation**	**pH / 40°C**	**TA**	**DIC**	**pCO_2**
Sample	(day)	(°C)		(mM)	(mM)	($x10^{-3}$ bar)	(day)		(mM)	(mM)	(bar)
blank 2	11	13.5	7.35	2.51	2.47	1.93	1	4.62	2.83	38.8	1.76
JdF mix 1	11	13.5	7.35	2.51	2.47	1.93	1	4.63	2.66	35.5	1.62
JdF mix 2	11	13.5	7.35	2.51	2.47	1.93	1	4.62	2.58	35.3	1.60
JdF mix 3	11	13.5	7.35	2.51	2.47	1.93	1	4.67	2.95	36.3	1.63
blank 3	24	16.2	7.69	2.46	2.17	0.75	3	4.79	2.91	27.8	1.22
MAR-A	23	16.2	7.69	2.32	2.17	0.75	2	4.81	2.83	26.0	1.13
G1	24	16.2	7.69	2.32	2.17	0.75	3	4.86	3.10	25.7	1.10
blank 4	13	15.0	7.64	2.46	2.32	0.91	3	4.74	3.05	32.4	1.43
JdF mix 2bis	13	15.0	7.64	2.46	2.32	0.91	3	4.78	2.98	29.1	1.28
MAR-Abis	13	15.0	7.64	2.46	2.32	0.91	3	4.76	2.80	29.1	1.29
MAR-B	13	15.0	7.64	2.46	2.32	0.91	3	4.77	2.97	29.6	1.30

Table 5: Rock dissolution extent in % using ΔSi and ΔCa concentrations for all the samples used during the experiment. Two cases are considered: “whole rock (WR)”, where all the rock is considered to be reactive, and “top-layer (TL)”, where only the topmost layer of ~5 g always in contact with the CO_2-rich solution is considered as reactive. All the aqueous concentrations are those collected on day 10.

	AQUEOUS SOLUTIONS		***WHOLE ROCK***			***TOP-LAYER***		
	ΔSi	**ΔCa**	**Mass** $_{WR}$	***Si*** $_{WR}$	***Ca*** $_{WR}$	***Mass*** $_{TL}$	**Si** $_{TL}$	**Ca** $_{TL}$
Sample	(mol)	(mol)	(g)	(%)	(%)	(all 5 g)	(%)	(%)
JdF mix 1	0.0004	0.0013	80	0.06	0.70	5	0.98	11.22
JdF mix 2	0.0003	0.0011	80	0.05	0.59		0.73	9.50
JdF mix 3	0.0004	0.0006	80	0.06	0.32		0.98	5.18
JdF mix 2bis	0.0002	0.0003	65	0.04	0.20		0.49	2.59
G1-A	0.0002	0.0007	80	0.03	0.29		0.53	4.62
MAR-A	0.0001	0.0002	80	0.02	0.11		0.24	1.73
MAR-B	0.0001	0.0001	30	0.04	0.14		0.24	0.86
MAR-Abis	0.0001	0.0001	65	0.02	0.07		0.24	0.86

Table 6: Summary of experimental conditions of current study and previous works.

	Reactor setup	**T**	**pCO_2**	**DIC**	**pH**	**Phases**
		°C	bar	mM		
This study	batch, seawater	40	1	<40	4.8	crystalline mafic rocks
Critelli et al. (2014)	mixed flow	25	-	-	2 - 12	metabasalt
Wolff-Boenisch et al. (2011)	mixed flow, seawater	25	4	114	3.5	basaltic glass, crystalline basalt, peridotite
Gislason and Oelkers (2003)	mixed flow	25 - 50	-	-	2 - 12	basaltic glass
Gudbrandsson et al. (2011)	mixed flow	5 - 75	-	-	2 - 11	crystalline basalt

FIGURES

Figure 1: Experimental setup for the CO_2-seawater-oceanic rock dissolution experiments. The crosses at the bottom of the HDPE bottle represent the ground sample. The CO_2 continuous inlet flux starts from the cylinder, where it is controlled by a standard gas regulator, continues through an on/off gas valve that further regulates the CO_2 flux, and enters into the reaction vessel, where it is homogeneously dispersed within the solution with a bubbler.

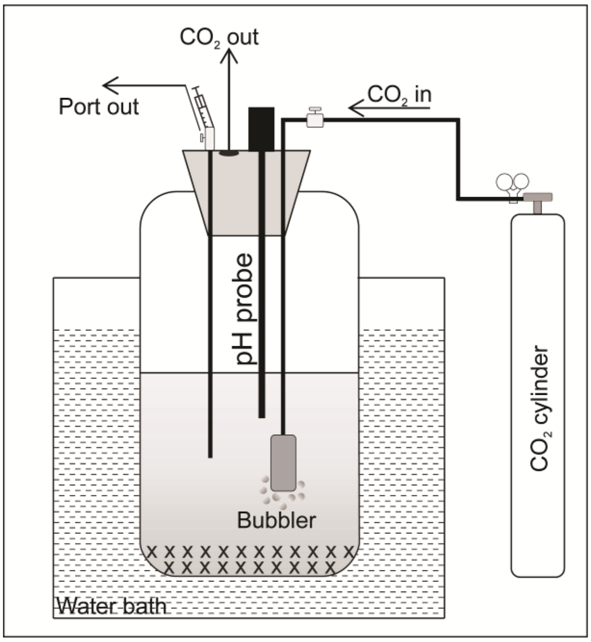

885 **Figure 2**: pH (a), total alkalinity (b) and DIC (c) trends throughout all the duration of the experiments. The pH has been measured *in situ* at 40 °C. For each run, the first output refers to the measurement taken at time “zero”, just before adding the solid sample, when the seawater is CO_2-saturated. All the reference solutions are shown in shades of blue and identified as blank 2, 3, and 4, respectively.

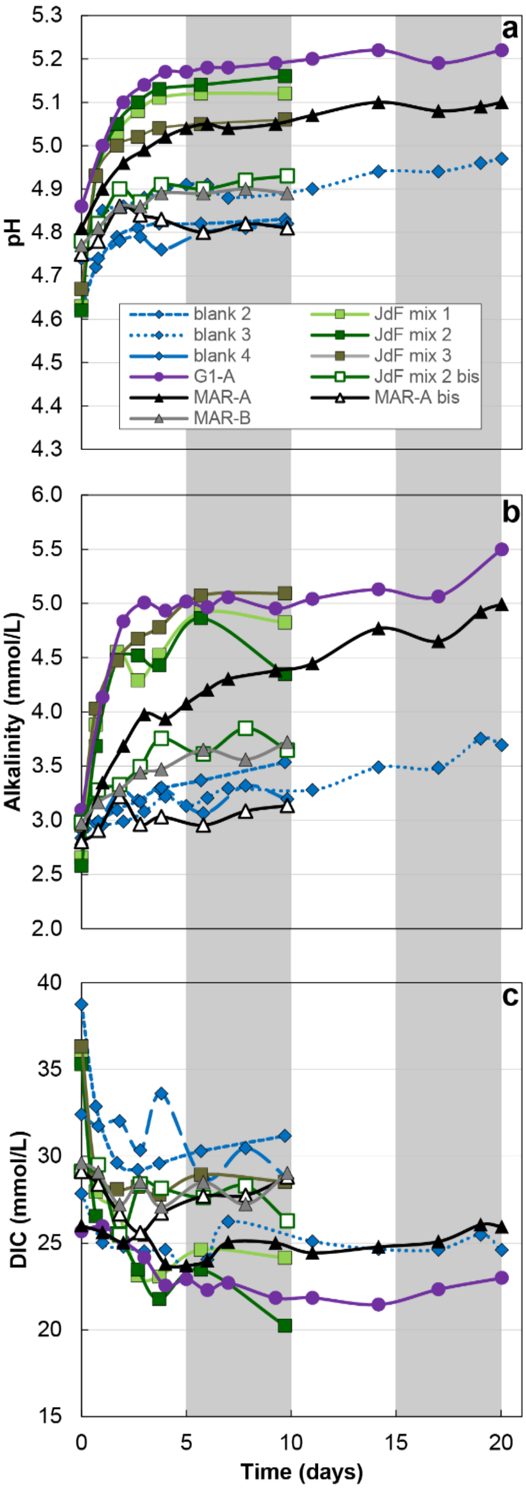

890

Figure 3: Si (a) and Ca (b) concentrations, together with Ca/Si (c) and ΔCa/ΔSi (d) ratios overtime during the dissolution experiments. In plots a and b, error bars represent the average 1σ (0.060 and 0.19 mmol/L for Si and Ca, respectively). In plots c and d, the rock stoichiometric ratio is indicated with a red line. For each run, the first output refers to the measurement taken at time “zero”, just before adding the rock, when the seawater is CO_2-saturated. All the reference solutions are shown in blue and identified as “blank”.

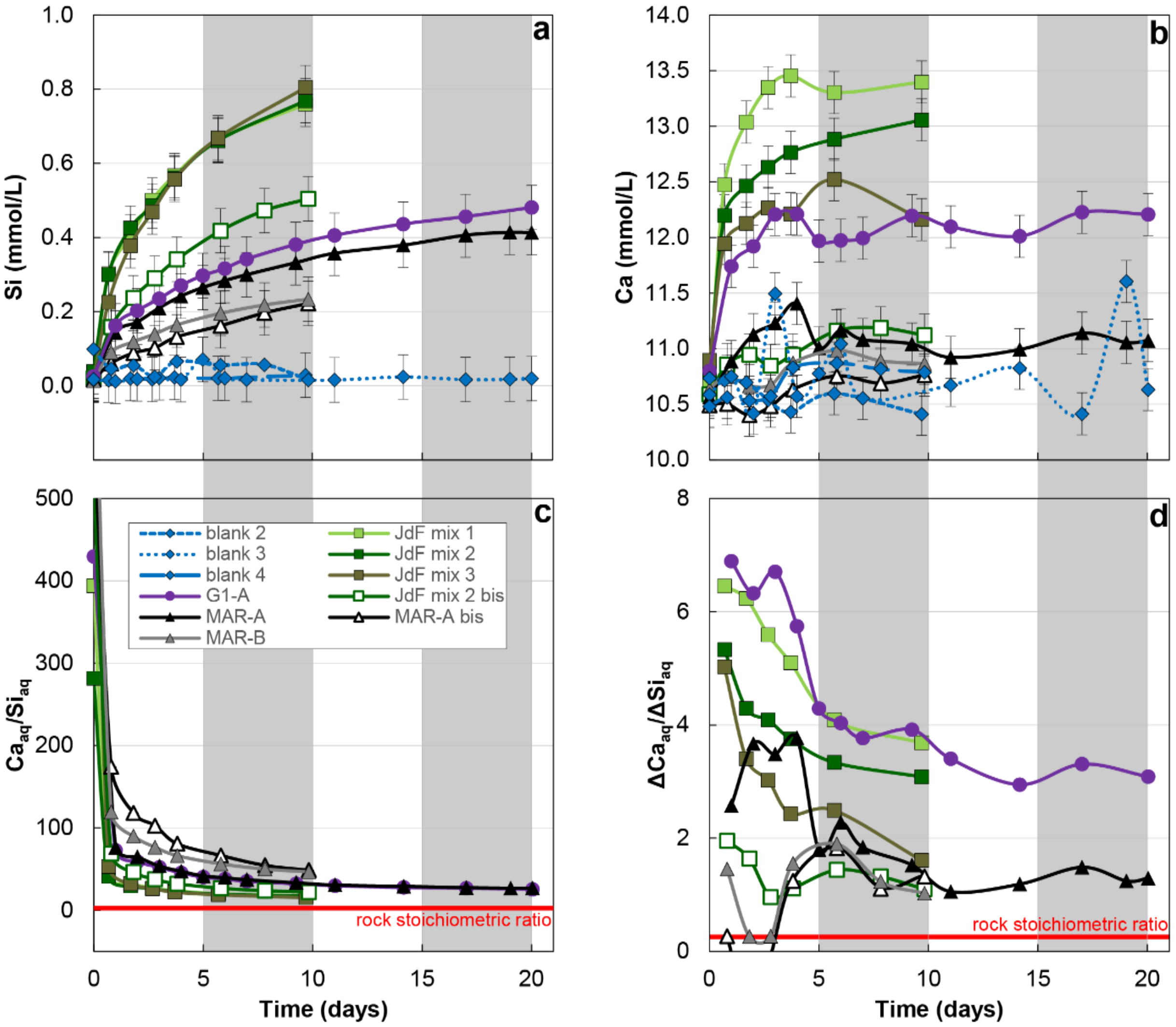

Figure 4: Grain size distribution analyses and SEM images for all the samples, before and after the experiments (pre and post, respectively). The SEM images were taken with 500x of magnification.

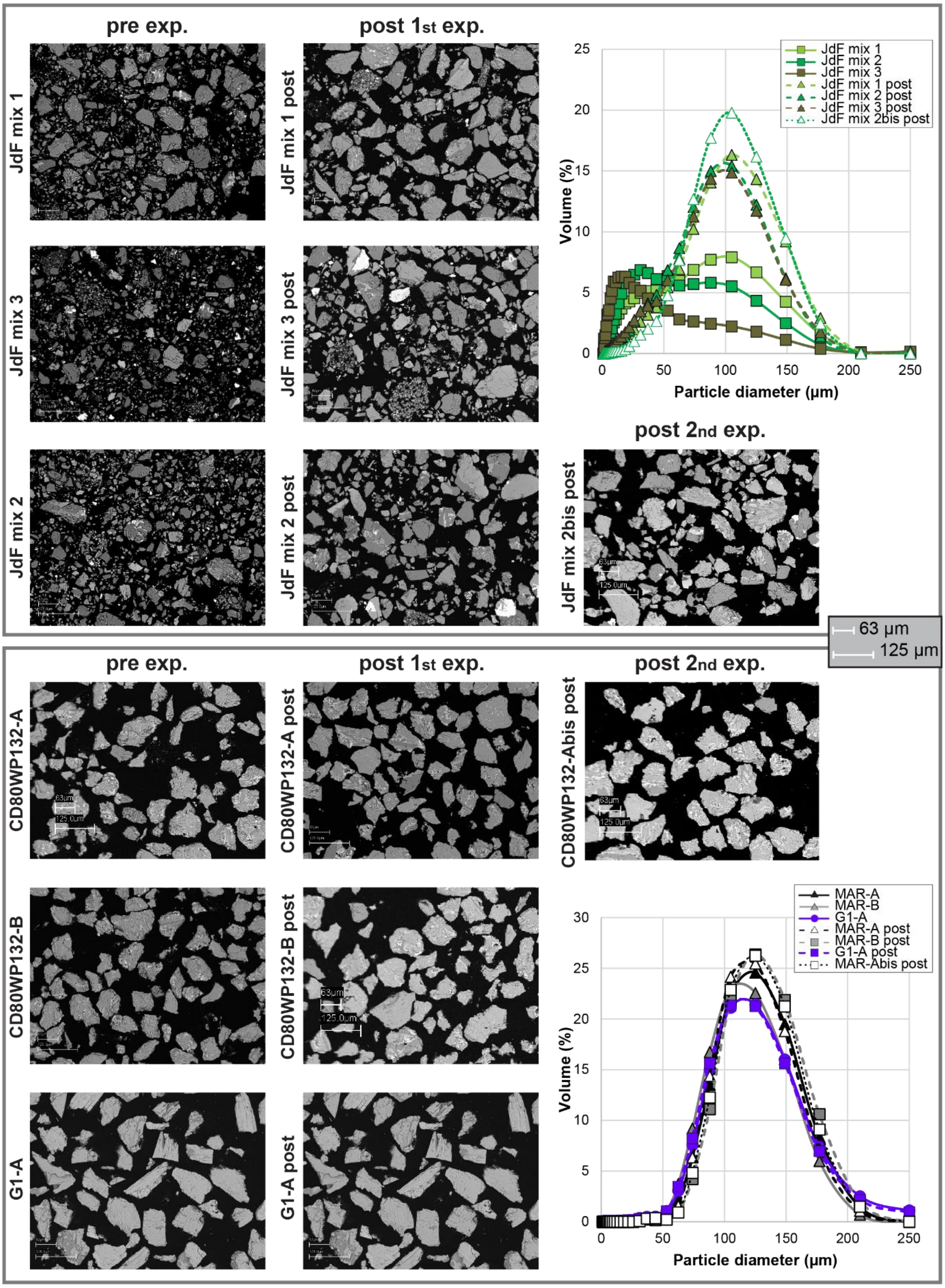

Figure 5: Si (a) and Ca (b) release rates as a function of time normalized to the initial geometric surface area of rock for all experimental runs. Ca release rates for MAR-Abis (days 0.8, 1.8, and 2.8) and MAR-B (days 1.8 and 2.8) have not been plotted due to analytical errors. Error bars (Si) or size of symbols (Ca) correspond to a ±0.24 or ±0.01 log unit estimated uncertainty calculated from the precision of Si and Ca concentrations measurements, respectively.

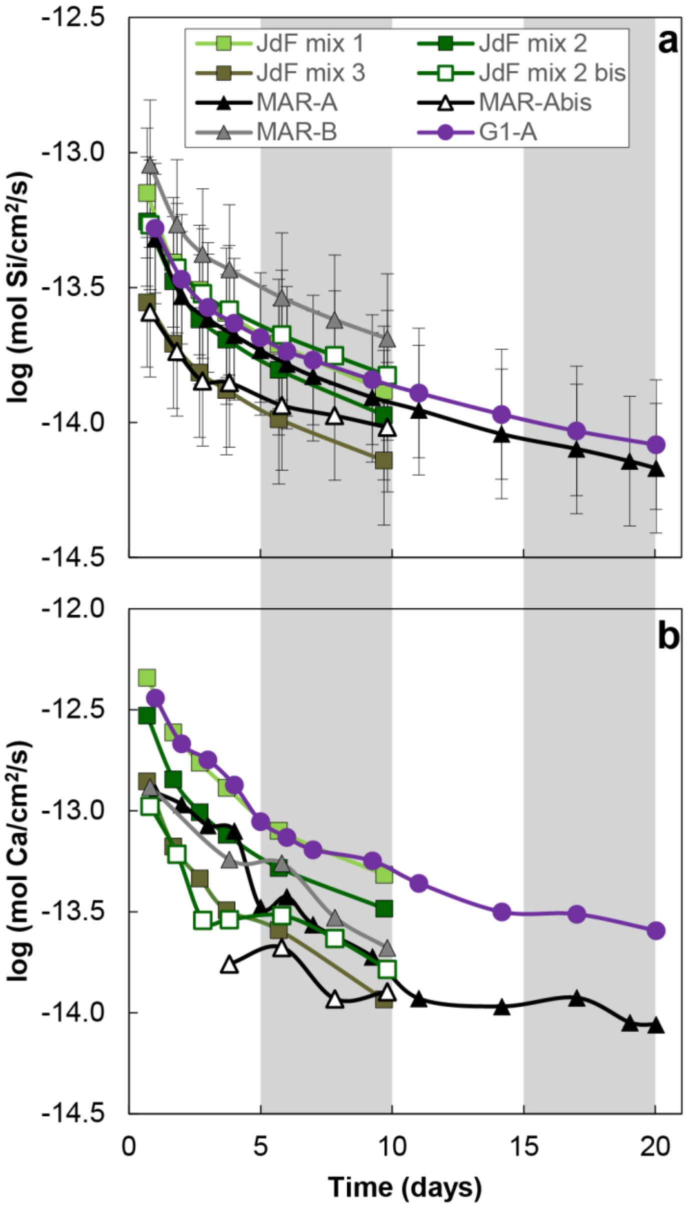

Figure 6: Si and Ca release rates normalized for the geometric surface area as a function of pH, for all the experimental runs of this study at 40 °C considering (a) the whole rock mass or (b) only the 5g top-layer, as shown by the additional explanatory sketches. Error bars (Si) or size of symbols (Ca) correspond to a ±0.24 or ±0.01 log unit estimated uncertainty calculated from the precision of Si and Ca concentrations measurements, respectively.

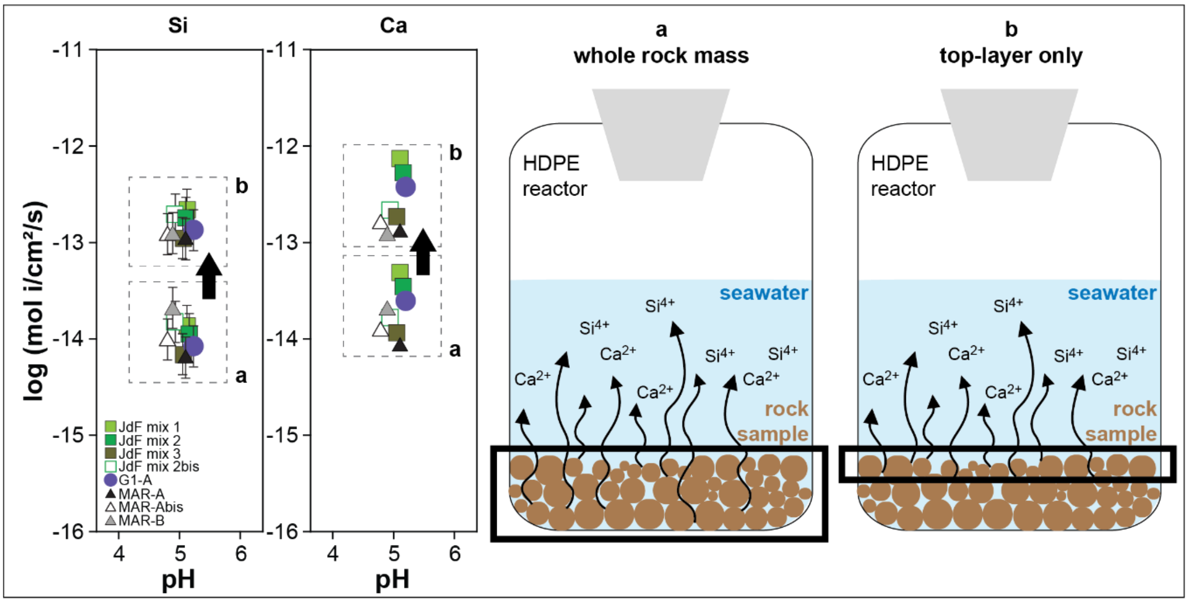

Figure 7: Si release rates normalized for the geometric surface area as a function of pH, for all the experimental runs of this study at 40 °C (coloured symbols: full colour for whole rock mass, shaded for top-layer only) and for SWC-Cl series from Wolff-Boenisch et al. (2011) at 25 °C, where G-basaltic glass, X-crystalline basalt, and P-peridotite. The blue lines indicate the overall dissolution rates proposed by Gislason and Oelkers (2003) for basaltic glass mixed-flow experiments at 25 and 50 °C as a function of pH, based on multioxide dissolution model. Error bars correspond to a ±0.24 log unit estimated uncertainty calculated from the precision of Si concentrations measurements.

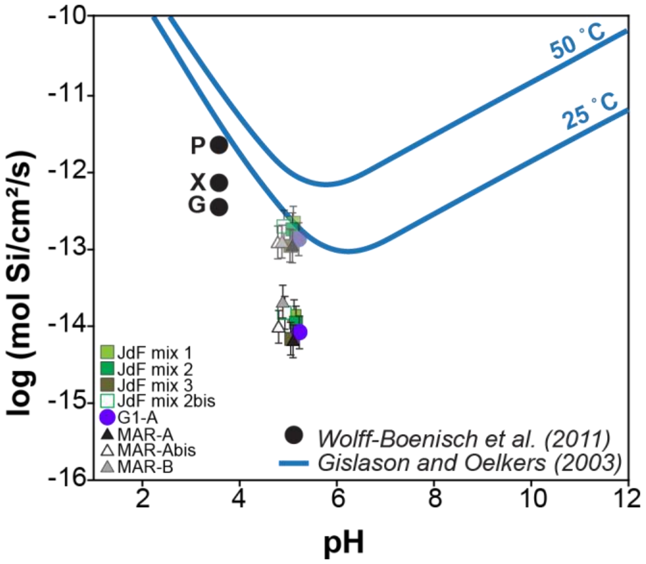

Figure 8: Si release rates normalized for geometric surface area for all the experimental runs as a function of pH (coloured symbols: full colour for whole rock mass, shaded for top-layer only), compared to experimental results of Critelli et al. (2014), Gudbrandsson et al. (2011), and Wolff-Boenisch et al. (2011) at 25 °C. The forsterite, diopside, albite, and hornblende rates at 25 °C illustrated in this figure are taken from Rimstidt et al. (2012), Knauss et al. (1993), Chou and Wollast (1985), and Golubev et al. (2005), respectively. The labradorite curve was taken from Gudbrandsson et al. (2011), who in turn obtained it multiplying the albite dissolution curve of Chou and Wollast (1985) by 4 to fit the bytownite and andesine rate data taken from Oxburgh et al. (1994). Error bars correspond to a ±0.24 log unit estimated uncertainty calculated from the precision of Si concentrations measurements. The rates for plagioclase, horneblende and metabasalt are shown as normalized to BET because geometric surface area cannot be calculated with the published data provided by the authors.

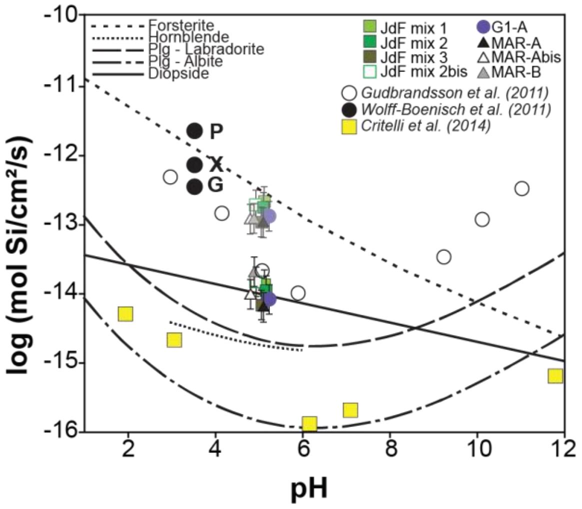

Figure 9: Ca release rates normalized to geometric surface area for all the experimental runs as a function of pH (coloured symbols: full colour for whole rock mass, shaded for top-layer only), compared to the experimental results of Gudbrandsson et al. (2011) at 25 and 50 °C renormalized for the geometric surface area. Size of symbols correspond to a ±0.01 log unit estimated uncertainty calculated from the precision of Ca concentrations measurements.